Editorial Manager(tm) for Boundary-Layer Meteorology
Manuscript Draft

Manuscript Number:

Title: A Motion Stabilized W-band Radar for Shipboard Observations of Marine Boundary Layer Clouds

Article Type: ISARS Special Issue

Keywords: Keywords W-band cloud radar, marine boundary layer clouds, motion stabilization, VOCALS 2008

Corresponding Author: Kenneth Moran

Corresponding Author's Institution: Univ of Colorado

First Author: Kenneth Moran

Order of Authors: Kenneth Moran;Sergio Pezoa;Christopher Fairall;Thomas Ayers;Alan Brewer;Christopher Williams;Simon de Szoeke

Abstract: Abstract A 94 GHz (W-band) radar suitable for use on shipboard studies of clouds has been developed. Cloud radars at X, Ka and W-bands have been used in the past for ocean studies of clouds, but the lack of suitable stabilization has limited their usefulness in obtaining accurate velocity measurements of the cloud particles and the heights of cloud features. A stabilized radar platform has been developed that is small and lightweight and can maintain the radar's beam pointing in the vertical to reduce the affects of the pitch and roll of the ship. A vertical velocity sensor on the platform allows the ship's heave effects to be removed from the measured cloud particle air speeds. Results from the VOCALS 2008 field program on the NOAA vessel Ronald H. Brown demonstrate the improvements to the cloud measurements after the ships motion effects are removed. The compact design of the radar also makes it suitable for use in aircraft studies. The radar is being repackaged to fit in an aft bay of a NOAA P3 aircraft to observe sea spray profiles during ocean storms.

Suggested Reviewers: Pavlos Kolias

James Mead

Peter May

Bruce Albrecht

Brad Orr

Ed Luke

# A Motion Stabilized W-band Radar for Shipboard Observations of Marine Boundary Layer Clouds

**Moran K., S. Pezoa, C. Fairall, T. Ayers, A. Brewer, C. Williams, and S. de Szoeke**

K. Moran (corresponding author), C. Williams
Cooperative Institute for Research in the Environmental Sciences. University of Colorado, Boulder, CO, USA
Email: ken.moran@noaa.gov
Phone: 303 497 6575
Fax: 303 497 6181

S. Pezoa, C. Fairall, T. Ayers
NOAA Earth System Research Laboratory/PSD, Boulder, CO, USA

A. Brewer
NOAA Earth System Research Laboratory/CSD, Boulder, CO, USA

S. de Szoeke
Oregon State University, Corvallis, OR, USA

**Abstract** A 94 GHz (W-band) radar suitable for use on shipboard studies of clouds has been developed. Cloud radars at X, Ka and W-bands have been used in the past for ocean studies of clouds, but the lack of suitable stabilization has limited their usefulness in obtaining accurate velocity measurements of the cloud particles and the heights of cloud features. A stabilized radar platform has been developed that is small and lightweight and can maintain the radar's beam pointing in the vertical to reduce the affects of the pitch and roll of the ship. A vertical velocity sensor on the platform allows the ship's heave effects to be removed from the measured cloud particle air speeds. Results from the VOCALS 2008 field program on the NOAA vessel *Ronald H. Brown* demonstrate the improvements to the cloud measurements after the ships motion effects are removed. The compact design of the radar also makes it suitable for use in aircraft studies. The radar is being repackaged to fit in an aft bay of a NOAA P3 aircraft to observe sea spray profiles during ocean storms.

**Keywords** W-band cloud radar, marine boundary layer clouds, motion stabilization, VOCALS 2008

## 1 Introduction

The dynamics and micro-physical properties of cloud droplets within marine stratocumulus boundary layer clouds are basic to understanding the role clouds play in air-sea interaction and their influence on radiative processes (Stephens et al. 1990). Shipboard cloud studies over the ocean off the coast of western Chile have taken place during the last decade to better characterize the dynamics of marine boundary layer clouds and to provide new data sets that can lead to improved modeling of the radiative process. Millimeter wavelength cloud radars in the Ka-band (35 GHZ) and the W-band (94GHz) have historically been used to measure the properties of the small cloud particles of non-precipitating and weakly precipitating (drizzle) clouds (Frisch et al. 1994; Mead et al. 1994; Kolias et al. 2007). Ka band radars have played an important role in measuring cloud properties from land based sites, where the radar physical properties such as size and weight are not a factor in the design. (Ackerman et al. 2003)

For mobile platforms such as ships and aircraft, the requirements for carefully engineered packaging as well as motion compensation beam steering place a demand on the size and weight of the radar (Li et al. 2004; Pazmany et al. 1994). To provide the sensitivity needed for land based cloud observing sites, Ka band radars used at the fixed field sites are typically characterized by large antenna diameters (2-4m) and integration times of several seconds. The smaller size and reduced weight of W-band cloud radars makes them better suited for shipboard as well as aircraft deployments. The wavelength dependence ($\lambda^{-4}$) of radar cross section offers a 17dB advantage to W-band radar over a similar Ka band design. This advantage can be used to provide performance suitable to mobile platforms without sacrificing sensitivity of the radar. Smaller antennas at W-band with less mass make the task of beam steering more manageable. For mobile platforms short dwell times are often used (<1s) to reduce the effects of platform motion.

Independent measurements of the platform motion using external velocity sensors can be used to remove motion caused biases.

W-band radars became a tool for studying the small water droplets in clouds after the pioneering work by Lhermitte (1987, 1988, 1990, 2002). The application to cloud studies followed his work and radar systems at universities and government sponsored research facilities greatly expanded during the next decade. Along with numerous Ka band radars the community of cloud radar researchers used these two wavelengths to study cloud micro-physics to provide a greater understanding of the capabilities and limitations of the two wavelengths. (Sekelsky et al. 1996, 1999; Kolias et al. 2007)

The Atmospheric Radiation Measurement (ARM) program sponsored by the Department of Energy, fielded several Ka band millimeter wavelength cloud profiling radars (MMCR) starting in 1996 (Moran et al. 1998; Ackerman et al. 2003). The radars pointed vertically, ran continuously and unattended and provided a record of cloud particle dynamics derived from the Doppler spectrum of the backscattered signal. These radars were the cornerstone instruments along with a suite of other instruments designed to observe clouds. Later the ARM program added several W-band radars for deployment on their mobile facilities, as they were easily transported in smaller packages.

NOAA's Environmental Technology Laboratory developed its own version of the ARM MMCR and participated in the Arctic SHEBA field program in 1997-98. The radar later participated in several cruises including the NOAA Vessel *Ronald H. Brown*, for field experiments in 1999, 2001 and 2003 (Webster et al. 2002; Bretherton et al. 2004, Kolias et al. 2004). While that radar measured non-precipitating cloud types with excellent sensitivity and temporal and spatial resolution, the ship motion caused problems with measuring the cloud particle behavior. The pitch and roll of the ship caused the fixed radar beam to wander off vertical and the natural horizontal winds combined with the ship's forward motion induced errors into the vertical particle velocities. The radar's 2m antenna had a fixed mount and the RF electronics were mounted inside the operating container making it difficult to configure the radar for any type of motion compensation hardware. At one point, the entire sea container that is used to house the radar was under consideration to be tilted fore and aft and side-to-side with hydraulic risers to keep the

radar beam vertical. Although this would have been a marvelous place to work and sleep to avoid motion sickness, it proved too challenging an undertaking. There was a growing need for a cloud radar that could be easily configured for shipboard use that included motion compensation hardware.

In this paper we will describe a new seagoing W-band radar including design characteristics, sensitivity and calibration issues, motion stabilization and correction, and give some examples from the first field deployment. Plans for future work and a summary conclude the paper.

## 2 Radar Design and Characteristics

Beginning in 2006 NOAA's Physical Science Division of the Earth Systems Research Lab designed and developed a W-band radar suitable for studying marine stratocumulus boundary layer clouds from research vessels such as NOAA's *Ronald H. Brown*. The radar was completed in time to be part of the VAMOS Ocean-Cloud-Atmosphere-Land Study Regional Experiment (VOCALS-Rex) in October-November 2008 (Wood et al., 2010). The radar is housed in a modified sea container that is routinely used on cruises. A rooftop hatch allows for the installation of an antenna port with shroud and a low loss radome for weather protection. The electronics were designed to be in two separate packages: 1) a small light weight section that contains all the high frequency RF electronics including the transmitter, antenna, receiver and waveguide and 2) an electronics rack that houses the computers, intermediate frequency (IF) electronics and transmitter power source. The small RF section was designed to weigh less than 100 pounds and have a center of gravity near the geometric center of its support frame, 2'x2'x3'. These mechanical features provided suitable characteristics to design and build a small autonomous positioner that would compensate for the pitch and roll of the ship and keep the radar beam pointed vertically during the cruise. The antenna is 12 inches in diameter and the 1.7KW klystron amplifier used for the transmitter provides a sensitivity of -33 dBZ at 2 km, sufficient to detect marine stratocumulus boundary layer clouds. The time interval between successive beams is 0.3s to provide sufficient temporal resolution needed to accurately resolve the effects of the vertical motion of the ship.

Operation of a shipboard stabilized platform requires a design with a light weight RF section that contains the antenna, transmitter and waveguide components that can be easily steered by a motion stabilizer (Fig. 1). The stabilizer is in the form of a cradle with two orthogonal rocking axes that can easily swing back and forth and side to side to compensate for the pitch and roll of the ship. The entire RF section and antenna is housed in an open frame for easy access and is balanced near the geometric center of the frame while resting in the support cradle of the stabilizer. The light weight and small size allowed for a robust design of the control system for the stabilizer. The stabilizer's control system works independently of the radar with its own PC based PID (proportional-integral-derivative) controller.

The radar electronics were separated into the high frequency RF section at 94.56 GHZ and the lower IF frequency sections at 2160 and 60 MHz (Fig. 2). The RF electronics include: 1) up converter from 2160 MHz to 94.56 GHZ, 2) transmitter driver circuits, 3) extended interaction klystron (EIK) amplifier,4) high voltage power supply and modulator, 5) output detection and protection circuits, 6) antenna, 7) waveguide switches (circulators) used for receiver protection, 8) low noise amplifiers and calibration noise source and 9) down converter to 2160 MHz. All of the RF electronics are mounted in a tubular frame supported by the cradle in the beam stabilizer.

The self enclosed transmitter unit contains the RF driver circuits, the EIK amp, the high voltage power supply/RF modulator and the output detection circuits. The EIK is protected from a mismatched output with a high power isolator as well as a feedback circuits that will place the transmitter into standby for a single pulse mismatched high power reflection.

The electronics for the intermediate frequencies (2160 and 60 MHz) and the remaining radar components are in a floor-to-ceiling rack and connected to the RF section through several small cabling harnesses. The rack contains the low voltage power supply and controller for the transmitter, the IF coherent up and down converter, the receiver switch control unit, the transmitter pulse display scope, the radar processor PC, the radar data management PC and the dual UPS systems for clean power.

*Lapxm* software from Vaisala provides modulation control of the transmit pulse and sampling control of the receiver. A digital IF receiver, the PIRAQ III from NCAR/

Vasiala samples the return signal at the 60 MHz IF and performs digital down conversion and filtering to baseband. Signal processing software computes an FFT Doppler power spectrum for each range gate and the first three moments are estimated using conventional methods (Kolias et al. 2005). Hourly spectra and moments files are saved (in netCDF) to an external spectra disk at the rate of about 20 GBytes per day. Mean power estimates are converted to reflectivity through the calibration software and moment and reflectivity files are sent hourly to the data management PC where they are archived.

The stabilized platform and the radar electronics work independently. A Kongsberg ship motion sensor outputs its measurements to the platform stabilization controller as well as to the data management PC for archiving. The GPS clock synchronization hardware maintains the data archive system clocks on the PCs to better than 0.1 s accuracy. A LabView radar monitor software package archives the radar error status along with the calibrated transmitted power on a ten minute interval.

The antenna is one of a set of three identical units designed for NOAA in 1992 as part of a microwave scintillometer. The units had been in storage for many years and their feeds and sub-reflectors were re-aligned and their antenna patterns measured when they were returned to Millitech for testing. All were found to be in excellent condition after alignment. The roof of the sea container that houses the radar has a 4' x 4' removable plate with a 3 foot diameter hole and a rolled edge shroud with a radome cover. The cover is made of shrink wrap material identical to that used to weatherize boats and marine gear. The one-way loss at W-band is less than 0.2 dB (private correspondence Pro Sensing).

The air cooled extended interaction klystron (EIK) amplifier provides a high power (1700 W peak) coherent power source, with low noise output and reliable operations for ten thousand hours or more. The transmitter includes output protection circuits and system monitoring for reliable operation from a 120 VAC power source. The IF-RF-IF coherent up/down converter can provide narrow output pulses of 100 ns and receiver bandwidths to 10 MHz for range resolution down to 15 m. A standard LNA with 5 dB noise figure is used in the receiver and provides sensitivity of -120 dBm for 25 m range resolution operation. A fixed bias 3-port circulator acts as a duplexer to isolate the

transmitter and received signals by 25 dB. The receiver protection switches (circulators) provide 25-30 dB of isolation at each stage in the receiver chain providing an additional 90 dB of protection from the transmitted pulse sequence. The antenna (Cassegrain design) has about 46 dB gain with $0.7^{o}$ beamwidth and sidelobes -18 dB below the main beam. The radar's digital IF receiver and processor uses 14 bits of sampled signal resolution and digital down conversion hardware that provides base band signals for Doppler processing. A special module was developed for the radar processor software that provides calibrated reflectivity and produces netCDF output files.

The quality of the output products provided by the radar dependents on 1) the fidelity of the transmitted signal, 2) a receiver with low noise and distortion and 3) signal processing hardware and software that can accurately estimate the moments of the Doppler power spectrum with minimal influence from artifacts. An end-to-end test of the radar, without the antenna, was used to characterize the processed return signals. A roughly calibrated sample of the transmitted signal was attenuated and injected into the LNA. After down conversion it passed through a 2 GHz delay line (15 μs) and into the digital IF signal processor. The plots in Fig. 3 show the received power, the signal-to-noise ratio and the noise level (in log units proportional to the ADC input voltage counts, dBi), versus RF input signal (dBm). The received power curve is extremely linear, better that 0.1 dB, for the range of signals up until saturation begins at about -41 dBm. The weakest detectable signals are better than -115 dBm and provide a linear dynamic range over 70 dB. The signal-to-noise ratio (SNR) is linear up until an input signal level of about -55 dBm at which point small non-linearities in the analog and digital IF receiver circuits start to introduce harmonics into the power spectrum. The noise estimate starts to increase significantly at this level while the SNR flattens out. The apparent rise in the noise is due to the signal leakage in the FFT that is normally suppressed by the Hanning window for small signals. A received signal level of -55dBm would correspond to an echo from a +27 dBZ cloud at 2 km. This level is near the upper limit for W-band non-Raleigh scattering measurements, typically in the range of 25-30 dBZ.

An example of a single spectral profile from a drizzle cloud during the VOCALS cruise is shown in Figs. 4a - b. The left panel (4a) shows a velocity-height profile with pseudo-color reflectivity (see section 5 for further discussion). Horizontal bars at each

height represent the spectral width while asterisks indicate the mean velocity. In Fig. 4b, 5 spectra separated by 250 m are shown. At heights of 500 m and 250 m, the spectra show separation into two distinct velocity regions forming individual peaks, indicative of differing drop size distributions.

# 3 Radar Sensitivity and Calibration

## 3.1 Sensitivity

An estimate of the radar's ability to detect weak clouds can be made by computing the minimum reflectivity as a function of height using the radar's characteristics and operational constants such as waveguide losses, antenna characteristics and transmitted power (Table 1 lists the radar characteristics during the VOCALS cruise and Table 2 the constants.)

To estimate the sensitivity at a particular range we compute the radar reflectivity from an estimate of the minimum detectable received signal (MDS) and a radar constant:

$$Z(dBZ) = MDS(dBm) + 20\log[R(m)] + RC\ (dB) \quad (1)$$

where $Z$ is reflectivity in dBZ, MDS is the estimated minimum detectable signal in dBm, $R$ is the range in meters and the radar constant ***(RC)*** in dB (for simplicity we have removed the physical units). The radar constant is derived from the Probert-Jones (1962) radar equation and takes the form:

$$RC = 10\log\left(\frac{512\ln(2)\lambda^2 10^{18} L_{SYS}}{P_T G^2 \theta\phi\Delta R\pi^3 K^2}\right) \quad (2)$$

Here λ = radar wavelength (m)

$L_{SYS}$ = System losses including matched filter loss (see Doviak and Zrnic, 1993)

$P_T$ = Peak transmitted power (milliwatts)

$G$ = Antenna one way gain – includes radome loss

φ = beamwidth (radians)

θ = beamwidth (radians)

$\Delta R$ = range cell depth (m)

$K^2$ = complex index of refraction for water at 20 $^{o}$C

Using the values from Table 2 the radar constant during the VOCALS cruise was, *RC*= 19.6 dB. The estimate of the minimum detectable signal is obtained from the radar operating temperature, receiver bandwidth and the threshold for signal detection:

$$MDS = k\,T_{OP}\,B_{NE}\,SNR_{Min}\,10^{\circ} \qquad (3)$$

where the MDS is in units of milliwatts

k = Boltzman's constant

$T_{OP}$ = radar receiver's operating temperature in K

$B_{NE}$ = Noise equivalent bandwidth of the of the receiver in Hz

$SNR_{min}$ = signal to noise ratio threshold for minimum detectable signals.

The radar operating temperature can be computed from the receiver noise figure, $F_n$, $T_{OP} = 290 \bullet F_n$. The noise equivalent bandwidth, $B_{NE}$, is related to the characteristics of the receiver bandwidth filter and the number of transmitted pulses that are coherently integrated (*NCI*) by the signal processor: $B = B_{NE}/\,NCI$. The W-band radar doesn't use coherent pulse integration and therefore *NCI* =1.

There are several techniques to estimate the threshold of signal detection using the SNR. The $SNR_{min}$ can be measured from the threshold of detected cloud data or by using an estimate from the SNR receiver statistics. In earlier work that determined the SNR threshold to distinguish significant echoes in the Doppler power spectrum, Riddle (1989) provided an empirical relationship by observing clear air returns from a 50 MHz wind profiler:

$$SNR_{\,threshold} = \frac{25 \times \sqrt{NFFT - 2.3125 + \frac{170}{NPTS}}}{NPTS \times NFFT} \qquad (4)$$

where *NFFT* is the number of FFTs averaged to form the power spectrum and *NPTS* is the number of points in the FFT. While this threshold was meant to provide for a robust signal threshold, rather than a minimum detectable signal level, it was used for many years as a reasonable estimate. Using the values during VOCALS, this $SNR_{threshold}$ = -11.9 dB

We can also estimate the minimum SNR from the statistical properties of a Doppler power spectrum (see Appendix A). From this estimate $SNR_{Min}$ can be written in terms of the *NPTS* and *NFFT*, similar to Riddle,

$$SNR_{Min} = \frac{a}{NPTS\ \sqrt{NFFT}} \qquad (5)$$

where *a* is a threshold factor for the signal to be greater than the standard deviation of the spectral noise. Here the VOCALS parameters yield a SNR threshold of -21.7 dB

To evaluate the threshold for VOCALS data we found a clear sky period and looked at the histogram of the SNR, Fig. 5. Using Fig 5 as a guide to comparing the thresholds from different estimates, the threshold value of -21.7 dB from the Appendix appears too sensitive and will generate a significant number of false hits. The Riddle estimate, which is near the far end of the scale appears not sensitive enough in this case and will miss a significant number of cloud detections. The mean SNR in Fig 5 is -20.3 dB and 2 standard deviations away, where there is only a small influence from noise, the threshold would be -17.9 dB. This threshold is 6.0 dB more sensitive than Riddle estimate of -11.9 dB. Using eq(5), we can compute the value of '*a*' for these three threshold estimates, where *NPTS* = 128 and *NFFT* = 8, which are shown in Table 3.

Finally, using the SNR threshold of -17.9 dB, the minimum detectable reflectivity $Z_{min}$(2km) is -33 dBZ, as shown in Table 1 column 2. We can compare the sensitivity of the ARM MMCR to the NOAA W-band radar if we use simulated operating characteristics of the W-band that match those of the ARM radar. The ARM's MMCR's has 7dB more antenna gain while using lower loss waveguide components (+2dB) and processes more pulses (+3dB). These operating advantages are offset by the 17 dB

advantage of operating at a shorter wavelength. The curves in Fig 6 show the computed sensitivity profiles with height for three radar configurations. The curves' shape follow the range squared dependence for reflectivity. For the VOCALS cruise the green curve in Fig 6 can be used, which has the same sensitivity as for aircraft flights. Here the reflectivity estimates range from better than -50 dBz at a few hundred meters from the surface to about -29 dBZ at 3 km providing sufficient sensitivity to detect most marine stratocumulus clouds.

### 3.2 Calibration

Radar calibration usually takes two forms: an internal calibration of individual system components or an external calibration using a target with known radar cross section. The internal method is sometimes easier to achieve, however the additive error from each individual calibration can create a larger than desired overall calibration uncertainty. As we had access to reasonably good test equipment and reliable antenna pattern measurements of gain and beamwidth we were able to use the internal method for the initial radar calibration.

To provide accurate estimates of reflectivity, the radar's calibration requires individual calibrations of the system's components that make up the computation of the Radar Constant *(RC*), an accurate estimate of the distance to each range cell and a calibration of the received power at the output of the antenna (eq 1). The individual component's measurements can be carried out with lab test equipments and the range calibration is done with a delay line. The transmitted power is measured hourly and the reflectivity computations use the latest value.

Calibration of the radar's receiver is important in order to obtain a measure of the processed signal gain, $G_{RP}$, which is used to convert the power estimated by the processor, in units of ADC counts, into calibrated received power, in milliwatts. We have chosen the processed signal gain ($G_{RP}$) to be the ratio of the power measured by the processor ($P_{RP}$) to the receiver power at the antenna terminals *(P*), in milliwatts.

$$G_{RP} = \frac{P_{RP}}{P} \quad or\ rearranging\ in\ units\ of\ dB$$

$$P(dBm) = P_{RP}(dB) - G_{RP}(dB) \qquad (6)$$

where *P(dBm)* is the received power in dBm at the output terminals of the antenna equivalent to the power at the input to the LNA. We use a noise diode with known excess noise ratio (*ENR*) and inject this into the LNA at the front end of the RF down converter stages (Fig. 2). The output noise power of the diode, $N_D(dBm)$, can be computed from the ENR. The gain will be the difference, in dB, between the measured noise added by the diode and the calibrated diode noise power:

$$G_{RP}(dB) = N_{RP}(dB) - N_D(dBm) \qquad (7)$$

where $N_{RP}\ (dB)$ is the total added noise with the diode on, measured by the radar's processor. The signal processing software estimates the mean noise power in the spectrum using the method of Hildebrand and Sekhon (1974). The technique to measure the added noise uses the standard *Y* factor computation which relies on two measurements of the spectral noise, one with the diode on and one with it off. The measured noise added by the diode is

$$N_{RP} = (\overline{N}_{ON} - \overline{N}_{OFF}) \times NPTS \quad and \quad N_{RP}(dB) = 10\log(N_{RP}) \qquad (8)$$

$\overline{N}$ is the linear mean noise power per FFT point.

Using a receiver with a noise equivalent bandwidth, $B_{NE}$ , the noise power from the diode with noise temperature $T_D$ is

$$N_D = 10\log(k\,T_D\,B_{NE}) \qquad (9)$$

The temperature of the diode is

$$T_D = L\,T_0\,(10^{\frac{ENR_{dB}}{10}} + 1) + (1 - L)\,T_0 \qquad (10)$$

where $T_0$ is the ambient room temperature, $L$ is any loss between the diode and the LNA and $ENR_{dB}$ is the diode's excess noise ratio in dB.

Using this method we computed the gain through the receiver and radar processor to be 185.2 dB (Table 2). This closely matches the gain derived from the linear receiver power curve shown in Fig 3. We estimated the possible errors in each of the component's calibration, including antenna gain and beamwidths, waveguide losses and calibration of the noise source with a resultant uncertainty of 2 dB. This is usually an acceptable range for errors in the estimate of radar reflectivity. Future plans call for a field calibration of the radar using a target with know radar cross section. This is a preferred method as it reduces the number of component calibrations, however it still has a drawback as it must rely on atmospheric conditions that are favorable to make the tests.

## 4 Motion Stabilized Platform

Fixed beam cloud radars aboard a ship at sea will have the ship's motion embedded in the cloud-droplet velocity profiles measured by the radar. The roll and pitch motion of the ship tilt the beam from vertical so that horizontal motions, either atmospheric or due to the ship's forward speed, have a component along the radial beam direction producing a fluctuating offset in the velocities. Even during relative light sea conditions where pitch and roll are limited to less than $\pm 5^o$ over 5 seconds, the speed of the ship along with the prevailing winds broadens the velocity spectrum and induces a radial component of the horizontal wind into the vertical particle speed. A 10 $ms^{-1}$ wind and a $3^o$ tilt into the wind appears as a 52 $cms^{-1}$ bias in the vertical wind, where a $0.5^o$ tilt results in a bias of about 9 $cms^{-1}$. Small overall tilt results in manageable biases in the velocity profiles. The vertical motion of the radar platform due to the heave of the ship adds velocity errors to the measured particle fall speeds, even with a stabilized beam. A radar platform along with a

vertical motion sensor can provide error corrections to the measured radar velocity profile, when the beam's direction can be maintained at or near vertical.

The NOAA W-band radar's RF electronics and antenna are housed in a small stabilized platform which can compensate for the ship's pitch and roll using two independent axes. The Kongsberg sensor, which provides the pitch and roll measurements, also provides a measure of the radar's instantaneous vertical velocity which can be used to correct for the ship motion.

A detailed conceptual design for the cradle that supports the electronics frame is shown in the Solid Works CAD drawing in Fig 1. The platform is constructed of 3/8" anodized aluminum plate with buttress bracing for stability. Two DC servo motors with gear reducers provide the 2 axis motion that compensates for pitch and roll. A view of the stabilized platform with the radar electronics frame installed is shown in Fig. 7. The platform is elevated and is mounted on rigid stand attached to the floor of the container. A small plastic cylinder, shown in the figure, is lined with microwave absorber and acts as a safety shield which houses the antenna. The roof top hatch with a slanted top cylindrical 3 foot opening is covered with a low loss 7 mil white shrink wrap plastic which acts as the radome cover for the antenna. The opening is sufficient to allow for greater than $\pm 10^0$ tilt of the antenna. Moderate to heavy seas with pitch and roll greater than $10^o$ are considered very active and create problems in accurate operation of the stabilizer.

Attached to the base of the motion stabilized platform is the Kongsberg Motion Reference Unit (MRU-Z) with a two-axis rotational position/rate sensors and a separate heave sensor. The sensor is a three-axis solid state optical gyroscope that provides pitch and roll measurements to better than $0.15^o$ dynamic accuracy at an output rate of 100 Hz to the controller. A vertical velocity sensor in the MRU-Z provides accurate measurements of the vertical motion of the stabilized radar. A block diagram of the motion stabilizer (Fig. 8) shows the components for one of the two axis controllers (roll and pitch axis controls are identical). The motion controller computes an error signal, *e(t)*, which provides the correction signal to the driver amp. The feedback controller provides servo motors correction signals used to compute speed and brake control while the gear reduction unit drives the axle. Mechanical tilt limit switches for each axis are

used as inputs to the brake control software and disable the drive signals if the limits are reached. The Kongsberg MRU-Z sensor provides analog outputs for use in the 2-axis motion controllers as well as digital outputs used to archive the platform's pitch, roll and heave measurements. The Crossbow sensor attached to the ship via the elevated fixed stand provides digital data for the pitch and roll of the ship (not used in the control system but archived for reference).

The setup and control for each component is done through software on the laptop. The control algorithm maintains vertical by comparing the measured roll or pitch position with the command position, which is the position when the antenna is in vertical. The command vertical position (0,0) is offset with the difference between the gravitational vertical vector measured by the MRU-Z and the antenna's vertical beam position. The antenna's beam direction was measured at an antenna test facility and is referenced to its mounting plate. The mechanical offset between the gravity vector and the vertical beam is typically less than $0.2^{o}$. The PID (proportional, integral and derivative) controller is used in a standard configuration to provide smooth control with minimal vertical offset, limited overshoot and fast response time. The 2-axis PID motion controller uses digital input-output control formats and the ADC (analog-to-digital converters) and the DAC (digital-to-analog converters) convert between the digital and analog control signals. The PID motion control is performed through adjustments to the gain setting for each function: *Kp, Ki,*and *Kd*. Proportional control improves response time, integral control eliminates steady-state errors and derivative control improves overshoot. During the initial sea trials on the VOCALS cruise the control parameters were adjusted until satisfactory response was achieved for the varying seas conditions. Adjusting the control parameters was required as the sea conditions changed.

# 5 Field test during VOCALS

### 5.1 Stabilized Platform Operations

In the fall of 2008 the VOCALS field experiment was conducted off the west coast of Chile to make measurements of the marine cloud environment using PSD's new W-band radar aboard the NOAA vessel *Ronald H. Brown*. The cruise had two separate legs with a

stop in Arica, Chile at mid point. On the first leg of the cruise the radar experienced a problem that caused some of the transmit pulse to leak into the receiver. This damaged the LNA resulting in significant loss of sensitivity. During the layover in Arica the problem was corrected and the second leg of the cruise provided the first detailed shipboard measurements from a motion stabilized cloud profiling radar. Preliminary scientific results from the cruise that demonstrate the systems capabilities were presented at ISARS 2010 (Fairall et al. 2010).

The motion stabilized platform operated autonomously from the radar using two independent motion controllers for pitch and roll and its own PC for setup and control. As this was the first field test of the stabilizer there were several different control parameters sets, for pitch and for roll, that were tried in order to maintain stable operation under a variety of sea conditions. The objective of stabilizing the beam is to maintain minimal mean beam tilt with low standard deviation for the roll and pitch values. Fig. 11 shows a time series of the pitch and roll values from the Kongsberg sensor which is fixed to the underside of radar base plate and the Crossbow sensor which represents the ship's motion. The top two panels are the pitch (red) and roll (blue) of the radar platform and the bottom two are the ship motion. The ship's pitch, fore and aft, was far less active than the roll from side to side. The ship's roll varied up to near 5º while the pitch varied about 2º. The Crossbow's vertical alignment was no better than a few degrees with respect to the ship so the Crossbow mean beam tilt values are not calibrated to better than a few degrees. The standard deviation of the pitch and roll of the radar compared to the ship shows about a factor of 10 improvement for roll and about 5 for pitch during this hour. The mean values for the radar's beam tilt are accurate to within a few tenths of a degree. The Kongsberg vertical position is zeroed with respect to the leveled antenna thus eliminating the offset between the measured vertical gravitational vector of the Kongsberg and the antenna beam vertical.

The stabilizer was operating during the entire cruise but the radar operated at full sensitivity only during leg2 of VOCALS. Fig. 10 shows a color coded map of each hour of operation of the stabilizer for leg2, days 316 through 337 giving the operational status. There were times when the response was noisy (tan blocks) and times when there were mean tilts that were larger than a few tenths of a degree (yellow blocks). At other times,

the gain values ($K_P$, $K_I$, $K_D$) were poorly matched to the sea conditions and the corrections were over-driven, causing the system to hit the stops and remained locked (red blocks). Fig. 13 shows representative once a day samples of the mean tilt and standard deviation of the radar beam compared to the ship for pitch and roll. Depending on sea conditions some values of the control parameters worked better than others during portions of the cruise. For leg2 of the cruise the control parameters for the feedback algorithm were frequently adjusted with successful results about 89% of the time.

### 5.2 Cloud Observations

The radar provides estimates of the first three moments of the Doppler spectrum for each of the range volume samples: signal power or reflectivity ($0^{th}$), vertical velocity ($1^{st}$) and spectral width ($2^{nd}$). The full spectrum for each sample is recorded on a external disc, producing about 1 Gigabyte of spectral data each hour. Height coverage for the VOCALS cruise is from about 200m to 3km with range resolution of 25m and sampling times of 0.3 s (Table 1). The first gate is about 100 m higher than normal due to a minimum delay guard band installed as part of the repair in Arica.

Fig. 12, left panel, shows the color coded time-height moment plots for day 331 hour 7 GMT for the second leg of the cruise, where a marine cloud is capped at about 1.5 km. The internal structure of the cloud shows periods of very weak or nearly neutral convective activity in the regions of negative velocity along with regions of light drizzle or precipitation (positive velocity is towards the radar). The reflectivity shows banding typical of convective cell structure within the range between -10 to +10 dBZ over the cloud depth. Spectral broadening near the top in some regions suggests droplet distribution of many different particle velocities and sizes. The center panel (day 335) shows plots of a weak thin layer at the threshold of reflectivity levels near -36 dBZ typical of the clouds decks in the region. The velocity plot shows a mix of upward movement (warm colors) and slight downward regions in the thin layer, progressing to more upward motion activity as the depth increases. The reflectivity plot for day 319, right panel, shows the cloud development from pre-drizzle conditions of droplets through the development of drizzle. The velocity field shows a sudden updraft that appears to elevate the cloud top slightly prior to observing the stronger reflectivities. Significant

spectral broadening occurs as the updraft passes and the light precipitation occurs suggesting a strong change in the drop size distributions.

The velocity fields shown in Fig. 12 have been post processed to remove the effects of the vertical ship motion. The Kongsberg heave sensor is mounted under the antenna and is coaxial with the radar beam. The velocity can be corrected for the ship's motion by subtracting the vertical radar velocity measured during the radar dwell period. Fig. 13 shows the velocity field of the radar before and after the correction. Vertical striping that occurs in the lower panel is due to the ships heave.

A detailed example of spectra from a drizzle cloud during the VOCALS cruise is shown in Figs. 4. Fig. 4a (left panel) shows a Doppler velocity power spectra profile during the VOCALS cruise at 14 November 2008, 11:54:35.087 UTC. The right panel, shows the reflectivity at each range gate (with a 25-m resolution) and the left panel shows the reflectivity in each velocity bin using pseudo-colors. The spectra shown in Fig. 4a have been normalized so that the mean noise is constant with range to show the relative shape of the spectra with altitude. There are multiple peaks in the reflectivity spectra profile with two to five separate peaks observed below 0.5 km. Fig. 4b shows five Doppler velocity reflectivity spectra observed from 0.25 to 1.25 km in 250 m increments. The reflectivity spectra are normalized so that the mean noise is -40 dBZ (shown with a dashed line) and the maximum noise for each spectrum is shown with the solid black line. Two peaks are observed in the spectra at 0.25 and 0.50 km heights. A question to ask is: are these minimum reflectivities between the two peaks due to the first minimum in the Mie backscattering function of raindrops at 94 GHz? If they are, then the minimum in reflectivity corresponds to the backscattering from raindrops with approximately 1.5 mm diameters (Lhermitte, 2002). Since raindrops with 1.5 mm diameters have a surface terminal fall speed of nearly 5 $ms^{-1}$ and the minimum reflectivities occur in the spectra near 2 m/s downward velocities, then these droplet spectra at 0.25 and 0.50 km would need to be in an updraft of nearly 3 $ms^{-1}$. Since it is unlikely that these spectra are in a 3 $ms^{-1}$ updraft, these multiple peak spectra are not due to variations in the Mie backscattering function, but are due to multiple rain droplet size distributions falling with different fall speeds.

# 6 Future Work

In addition to surface-based observations of marine clouds, another application for NOAA's transportable W-band radar is for airborne observations of sea spray profiles of droplet distribution with height. This information is relevant to modeling the development of hurricanes. Small water droplets that are generated by winds and waves are carried aloft during storms and observing them with a nadir pointing W-band radar from an aircraft at 2 km altitude can be achieved if the radar's sensitivity is on the order of -20 dBZ. ESRL's Physical Science Division plans to operate the W-band radar in the aft bay of a NOAA P3 research aircraft. These aircraft make routine missions into storms at sea. We plan to make preliminary flight tests in the near future with the repackaged radar, followed by missions to collect storm data to estimate the distribution and size of sea spray with height.

Radars operating at W-band have been used for aircraft observations of clouds because of their favorable size, weight and high sensitivity to small water droplets (Pazmany et al. 1994; Li et al. 2004). Cloud measurements from an aircraft offers significant advantage over fixed based platforms as search patterns can be planned based on desired observations rather than the uncertain nature of a clouds available to a fixed platform. Routine observations of sea spray from a ship navigating through a strong storm are difficult at best and research programs designed to make those measurements have rarely been undertaken.

Airborne observations of sea spray using a nadir looking W-band radar have a much greater potential for success in making near-surface observations. Measurements of sea spray to profile the distribution of particle drop size characteristics with altitude would take place during a flight path that passed through the alternating bands of precipitating and clear regions in hurricanes. The clear regions will allow the radar to measure the return from sea spray without observing a mixture of sea spray and precipitation. The NOAA W-band radar with its present sensitivity is a useful tool for measuring the Doppler spectrum of the droplets concentrations with altitude to estimate reflectivity, vertical velocity and spectral width distributions with range. The proposed operating characteristics for the radar configured for use on a NOAA P3 aircraft is shown in Table

1- column 3. A project is underway to repackage the RF electronics in a pressure vessel suitable for flights in a P3.

A sea spray source function (Fairall et al. 2009) is used to compute height profiles of size concentrations of sea spray droplets as a function of horizontal winds. Larger particles have higher concentrations near the surface that decreases with altitude (Fig. 14). With an airborne radar, sensitivity to small droplets increases with altitude which matches the particle detection requirements in the model. From Fig. 6 at an altitude of 2km the sensitivity near the ocean surface is about -33 dBZ with the radar is operating using 18 m range gates and short interval times between beams of 0.2 s.

The NOAA P3 aircraft have an unpressurized aft bay that is suitable to house the radar. The present radar configuration that has been used on the ship deployments will be partially repackaged to reduce the volume of the RF electronics including the transmitter, antenna and receiver. The repackaged design will provide a pressure containment vessel to maintain internal pressure close to sea level altitude. The remaining electronics will be housed in electronics racks internal to the aircraft. This new configuration will be used on all future deployments, either sea or air. Fig. 15 is a conceptual drawing of the new configuration (courtesy of Pro Sensing Corp.). It shows the internal aircraft pressure dome with the radar RF electronics mounted on a plate and the antenna positioned to look downward (nadir) under the plate. No radar pressure vessel is shown and it will eventually be attached on the edge of the mounting plate. Underneath is the removable aircraft fairing used to protect the antenna when flying. This configuration can be used for ocean studies by removing the pressure vessel and repositioning the antenna from nadir view to a vertical view with minimal waveguide rerouting. The pressure vessel will be a closed air system with a chiller plate and cooling fins to provide air for the transmitter tube and to maintain the internal operating temperature.

# 7 Summary

NOAA's Physical Science Division has fielded a new motion stabilized W-band radar suitable for use aboard a ship for the study of marine boundary layer clouds. With 25-m range gates and a 0.3 s dwell time, the sensitivity of the radar at 2 km is -33 dBZ which

provides detailed structure of the non-precipitating and weakly precipitating clouds over regions of the ocean where studies of air-sea interaction are important in modeling radiatively significant processes. The radar uses a servo controlled 2-axis stabilizer to maintain the beam in the vertical and an integral velocity sensor to record vertical ship motion for post processing the velocity profiles to remove the effects of the ship's heave. Field tests during the VOCALS 2008 program demonstrate the effectiveness of the stabilization and the quality of the cloud measurements made using this new technique. Further applications of the new radar to the study of sea spray from an aircraft platform are underway and the radar's mechanical assembly is being engineered to fit the aft bay of a NOAA research aircraft for future flights in storms.

***Acknowledgments*** This work was partially funded by NOAA's Office of Global Programs, CPPA program element

## Appendix A

### Estimating a signal to noise threshold for signal detection using the statistics of the Doppler power spectrum

At a particular frequency, with Doppler frequency resolution Δf, spectral noise is

$$S_N = \langle S_N \rangle \pm \sigma_{S_N} \text{ where } \quad \sigma_{S_N} = \frac{\langle S_N \rangle}{\sqrt{NFFT}} \qquad (11)$$

*NFFT* is the number of FFTs averaged to form the power spectrum. The Doppler power spectral density, *S*, contains both the signal and the noise:

$$Signal = S_S = \int \left( S - \langle S_N \rangle \right) df \qquad (12)$$

$$Noise = \int \langle S_N \rangle \, df \; = \langle S_N \rangle \, \Delta f \, NPTS \qquad (13)$$

*NPTS* is the number of points in the FFT spectrum.

For a weak signal confined to 1 frequency bin to be detected it should be greater than the standard deviation of the spectral noise ($\sigma_{Noise}$) by some value '*a*' or

$$S_S = \left(S - \langle S_N \rangle\right) > a\sigma_{Noise} \qquad (15)$$

where *a* is defined by the probability function

$$PROB\left(S_S > a\sigma_{Noise}\right) \cdot NPTS \cong 1 \qquad (16)$$

This condition follows from the requirement that we only expect no more than one out of *NPTS* to exceed $\langle S_N \rangle$ *by* $a\sigma_{Noise}$.

If we assume a Gaussian shape to the signal-to-noise distribution, we can use a form of the error function, *erfc*, to estimate the probability that the signal exceeds $\langle S_N \rangle$ *by* $a\sigma_{Noise}$**:**

$$PROB\left(X > \kappa\sigma\right) = Q(\kappa) \quad where \quad Q(\kappa) = \frac{1}{2} erfc\, \frac{\kappa}{\sqrt{2}} \qquad (17)$$

From 17 we can compute the expected values of *a* for several FFTs.

For *NPTS = 128* $PROB\left(S_S > a\sigma_{Noise}\right) = 7.81 \cdot 10^{-3} = Q(a) \Rightarrow a \approx 2.45$

For *NPTS = 256* $PROB\left(S_S > a\sigma_{Noise}\right) = 3.91 \cdot 10^{-3} = Q(a) \Rightarrow a \approx 2.68$

Now

$$Signal = a\sigma_{Noise}\Delta f \qquad (18)$$

$$\frac{Signal}{Noise} = \frac{a\sigma_{Noise}\Delta f}{\langle S_N \rangle \Delta f\, NPTS} = \frac{a}{NPTS\sqrt{NFFT}} = SNR_{Min} \qquad (19)$$

Thus, we can find the expected minimum detectable signal threshold in terms of the signal-to-noise ratio in dB as $10\log SNR_{Min}$

For *NPTS = 128, NFFT = 8 and a = 2.45,* $SNR_{Min}$ = -21.7 dB

For *NPTS = 256, NFFT = 8 and a = 2.68,* $SNR_{Min}$ = -24.3 dB

**References**


Ackerman, T. P., and G. Stokes, 2003: The Atmospheric Radiation Measurement program. *Phys. Today*, 56, 38–45.

Bretherton, C. S., T. Uttal, C. W. Fairall, S. E. Yuter, R. A. Weller, D. Baumgardner, K. Comstock, and R. Wood, 2004: The EPIC 2001 Stratocumulus Study. *Bull. Am. Met. Soc*., 85, 967-977.

Doviak, R. J., and D. S. Zrnic, 1993: Doppler Radar and Weather Observations. Academic Press, 562 pp.

Fairall C. W., K. Moran, S. Pezoa, D.E. Wolfe, S. de Szoeke, and V. Ghate: A New Motion-Stabilized W-band (94-GHz) Cloud Radar for Observations of Marine Boundary-Layer Clouds. *Preprints of the ISARS Symposium*., Paris, Fr, 28-30 June, 2010 [http://www.isars2010.uvsq.fr; Paper *O-MEA/01*].

Fairall, C. W., M. Banner, W. Peirson, R. P. Morison, and W. Asher, 2009: Investigation of the physical scaling of sea spray spume droplet production. *J. Geophys., Res*., 114, C10001, doi:10.1029/2008JC004918.

Frisch, A. S., C. W. Fairall, and J. B. Snider, 1995: Measurement of stratus cloud and drizzle parameters in ASTEX with a Kα-band Doppler radar and microwave radiometer. *J. Atmos. Sci.*, 52, 788–2799

Hildebrand, P. H., and R. S. Sekhon, 1974: Objective determination of the noise level in Doppler spectra. *J. Appl. Meteor.*, 13, 808-811.

Kollias, Pavlos, C. W. Fairall, P. Zuidema, J. Tomlinson, and G. A. Wick, 2004: Observations of marine stratocumulus in SE Pacific during the PACS 2003 Cruise. *Geophys. Res. Lett*., 31, Art. No. L22110.

____, Eugene E. Clothiaux, Bruce A. Albrecht, Mark A. Miller, Kenneth P. Moran, and Karen L. Johnson, 2005: The Atmospheric Radiation Measurement Program cloud profiling radars: An evaluation of signal processing and sampling strategies, *J. Atmos. and Oceanic Tech*., 22, 930–948.

——, E.E.Clothiaux, M.A.Miller, B.A. Albrecht, G.L. Stephens, and T.P. Ackerman, 2007: Millimeter-wavelength radars - New frontier in atmospheric cloud and precipitation research. *Bull. Am. Met. Soc*., 88, 1608-1624

Lhermitte, R. M., 1987: A 94-GHz Doppler radar for cloud observations. .*J. Atmos. Oceanic Technol.*, 4, 36–48.

——, 1988: Observations of rain at vertical incidence with a 94 GHz Doppler radar: An insight of Mie scattering. *Geophys. Res. Lett.*, 15, 1125–1128.

——, 1990: Attenuation and scattering of millimeter wavelength radiation by clouds and precipitation. *J. Atmos. Oceanic Technol.*, 7, 464–479.

——, 2002: Centimeter and Millimeter Wavelength Radars in Meteorology. Lhermitte Publications, 550 pp.

Li, L., G. M. Heymsfield, P. E. Racette, L. Tian, and E. Zenker, 2004: A 94-GHz cloud radar system on a NASA high-altitude ER-2 aircraft. *J. Atmos. Oceanic Technol.*, 21, 1378–1388.

Mead, J., A. Pazmany, S. Sekelsky, and R. McIntosh, 1994: Millimeter-wavelength radars for remotely sensing clouds and precipitation. *Proc. IEEE*, 82, 1891–1906

Moran, K. P., B. E. Martner, M. J. Post, R. A. Kropfli, D. C. Welsh, and K. B. Widener, 1998: An unattended cloud-profiling radar for use in climate research. *Bull. Amer. Meteor. Soc.*, 79, 443–45.

Pazmany, A. L., R. E. McIntosh, R. Kelly, and G. Vali, 1994: An airborne 95-GHz dual polarization radar for cloud studies. *IEEE Trans. Geosci. Remote Sens*., 1, 731–739

Probert-Jones, J.R., 1962: The radar equation in meteorology. *Quart. J. Royal Meteorol. Soc.*, 88, 485-495.

Riddle, A. C., K. S. Gage, B. B. Balsley, W. L. Ecklund, D. A, Carter, 1989: Poker Flat MST Radar Data Bases. *NOAA Tech. Memorandum*, ERL AL-11.

Stephens, G. L., S. C. Tsay, P. W. Stackhouse, and P. J. Flatau, 1990: The relevance of the microphysical and radiative properties of cirrus clouds to climate and climate feedback. *J. Atmos. Sci*., 47, 1742–1752.

Sekelsky, S. M., and R. E. McIntosh, 1996: Cloud observations with polarimetrc 33 GHz and 95 GHz radar. *Meteor. Atmos. Phys.*, 59, 123–140.

——, W. L. Ecklund, J. M. Firda, K. S. Gage, and R. E. McIntosh, 1999: Particle size estimation in ice-phase clouds using multi-frequency radar reflectivity at 95, 33, and 2.8 GHz. *J. Appl. Meteor.*, 38, 5–28.

Webster, P. J., C. W. Fairall, P. W. Hacker, R. Lukas, E. F. Bradley, and S. Godfrey, 2002: The Joint Air-Sea Monsoon Interaction Experiment (JASMINE) Pilot study. *Bull. Am. Met. Soc.*, 83, 1603-1630.

Woods, R., and 32 coauthors, 2010: The VAMOS Ocean-Cloud-Atmosphere-Land Study Regional Experiment (VOCALS-REx): goals, platforms, and field operations. *Atmos. Phys. Chem. Disc*., http://www.atmos-chem-phys-discuss.net/10/20769/2010/acpd-10-20769-2010.html.

**Tables**

**Table 1** Characteristics for NOAA's W-band radar during VOCALS (col 2), proposed P3 aircraft sea spray study (col 3) and ARM's MMCR (col 4)

| Platform | Shipboard (VOCALS cruise) | NOAA P3 Aircraft (planned) | Land Based ARM MMCR |
|---|---|---|---|
| Application | Cloud Properties | Sea Spray | Cloud Properties |
| Frequency | 94.56 GHz | 94.56 GHz | 34.86 GHz |
| Peak/Avg Power | 1750/3W | 1750/1 W | 200/0.3W |
| Platform Altitude | Sea surface | 5k-10k ft (1.5-3km) | Earth surface |
| $PRF_{MAX}$ | 8.33 KHz | 10 KHz | 11.1KHz |
| Antenna | 12 in Cassegrain | 18 in Cassegrain | 72 in Cassegrain |
| Gain - beamwidth | 46 dB, ~0.7$^o$ | 48 dB, ~0.5$^o$ | 53 dB, ~0.3$^o$ |
| Antenna Beam Positioner | Pitch-Roll Compensation | None | None |
| Pointing Directions | Vertical | Nadir | Vertical |
| Polarization | No | No | No |
| Pulse Integration | No | No | 6 |
| Pulse Width | 167ns (PM), | 125ns (PM) | 292 ns |
| Range Cell Size | 25 m | 18.75m | 44m |
| Number of Ranges | 120 | 100 – 200 | 139 |
| Maximum Range | 3 km | 2.25 km | 6.1km |
| Velocity Resolution | 10.3 $cms^{-1}$ | 6.2 $cms^{-1}$ | 4.5 $cms^{-1}$ |
| Max Radial Velocity | ± 6.6 $ms^{-1}$ | ± 7.9 $ms^{-1}$ | ± 5.7 $ms^{-1}$ |
| Temp. Stabilized RF | No | Yes | No |
| Pressurized Enclosure | No | Yes | No |
| Signal Processing Time between beams | 128 pt FFT Nspec=8 ~0.3 s | 256 pt FFT NSpec = 8 ~0.2 s | 256 pt FFT NSpec = 20 ~1.5 s |
| Data formats | netCDF, Ascii | netCDF, Ascii | netCDF |
| Estimated Sensitivity (no atmos losses) | -33 dBZ (R = 2 km) | -33 dBZ (R = 2 km) | -37 dBZ (R=2 km) |

**Table 2** System constants for W-band radar during VOCALS

| | |
|---|---|
| $\lambda$ = wavelength (meters) | 3.17 mm |
| $L_{TX}$ = transmit path loss | 4.0 dB |
| $L_{RX}$ = receiver path loss | 2.2 dB |
| $L_{MF}$ = matched filter loss (See Doviak and Srnic, 1993) | 2.3 dB |
| $P_T$ = Peak transmitted power | 62.4dB |
| $G$ = Antenna one way gain – includes radome loss | 45.9 dB |
| $\theta - \varphi$ beamwidths | $0.76^o$, $0.70^o$ |
| Antenna near field distance ($2D^2/\lambda$) | 65m |
| $\Delta R$ – range cell height | 25m |
| $K$ – complex index of refraction of water | 0.712 @ $0^o$C<br>0.779 @ $10^o$C<br>0.828 @ $20^o$ C |
| Receiver Noise Figure, $T_{OP}$ | 5.0 dB, $917^o$K |
| Noise equivalent bandwidth | 6.24 MHz |
| Processed signal gain, $G_{RP}$ - calibrated | 185.2dB |

**Table 3** Three SNR threshold estimates from empirical methods (Riddle), spectral probability statistics (Appendix A) and SNR measurements

| SNR threshold method | Threshold (dB) | Value of a |
|---|---|---|
| Riddle | -11.9 | 23.38 |
| Appendix A | -21.7 | 2.45 |
| SNR statistics | -17.9 | 5.87 |

Figure captions

**Fig 1** Concept drawing of the two axes motion stabilizer with the radar frame resting in the cradle

**Fig 2** W-band radar block diagram – RF mounting frame (dash-dot-dot) and rack mount electronics

**Fig 3** Received signal characteristics: power, signal-to-noise ratio and mean noise from an injected sample of the transmitted signal (see text)

**Fig 4a** Color coded reflectivity contours of the Normalized Noise Doppler velocity spectra from a drizzle cloud during VOCALS 2008. Asterisks mark the mean velocity and short horizontal lines indicate spectral width. Range spacing is 25 m and dwell time is 0.3s

**Fig 4b** Doppler velocity spectra for 5 ranges separated by 250 m for the same cloud in 4a. The development of separate droplet velocity distributions can be traced as the cloud particles descend

**Fig 5** Histogram of SNR values for a clear sky used to estimate SNR threshold for cloud detection

**Fig 6** Profile of radar sensitivity in dBZ for the W-band radar operating in the ARM mode (blue solid), airborne W-band (green dots) and land based ARM cloud radar (red dash) The sensitivity profile for VOCALS is identical to the curve for the airborne radar (green dots)

**Fig 7** Photo of the stabilized platform with the radar frame resting in the cradle. The roof hatch with the slanted antenna radome is located above the cylindrical antenna shroud.

**Fig 8** Block diagram of the stabilized platform control system: two axis motion controller, driver amp with feedback control, servo motors with reduction gear, MRU-Z and Crossbow motion sensors.

**Fig 9** One hour time series of pitch and roll for the stabilized radar platform (upper 2 panels) and the ship (lower 2 panels)

**Fig 10** Color coded hourly status of stabilized platform during VOCALS 2008 (percentage of total) : Blue = turned off; Tan = noisy (7%); Yellow = bias (8%); Red = not stabilized (11%); Green = stabilized (74%).

**Fig 11** Mean tilt (dots-circles), STD ship (dashes-squares), STD radar (solid-triangles), from the daily samples of pitch (left panel) and roll (right panel)

**Fig 12 D**ays 331, 335, 319, left to right : reflectivity (upper panel), velocity (mid), spectral width (lower). Drizzle (left panel), thin low reflectivity layer (center), transition to convection and drizzle, right.

**Fig 13** Stabilized W-band radar velocity field: corrected for vertical ship motion (upper panel), without correction for ship motion (lower panel).

**Fig 16** Fairall-Banner model estimate of the height profile of radar reflectivity from sea spray generated by 40 m/s winds

**Fig 17** Concept CAD drawing of the W-band radar repackaging for the NOAA P3 research aircraft. The radar's RF section fits on a plate with transmitter tube (red) and 12" dish mounted in a nadir position underneath. The aircraft's fuselage is shown in transparent gray and aircraft fairing in transparent blue

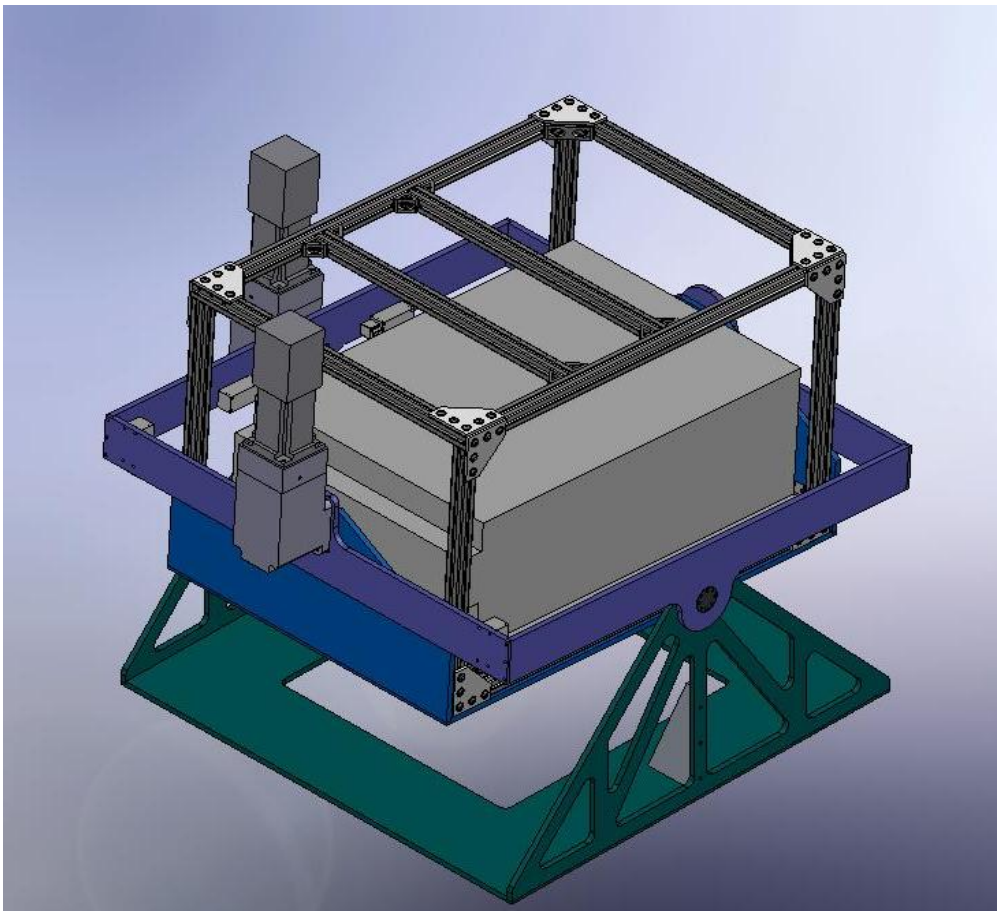

**Fig 1**

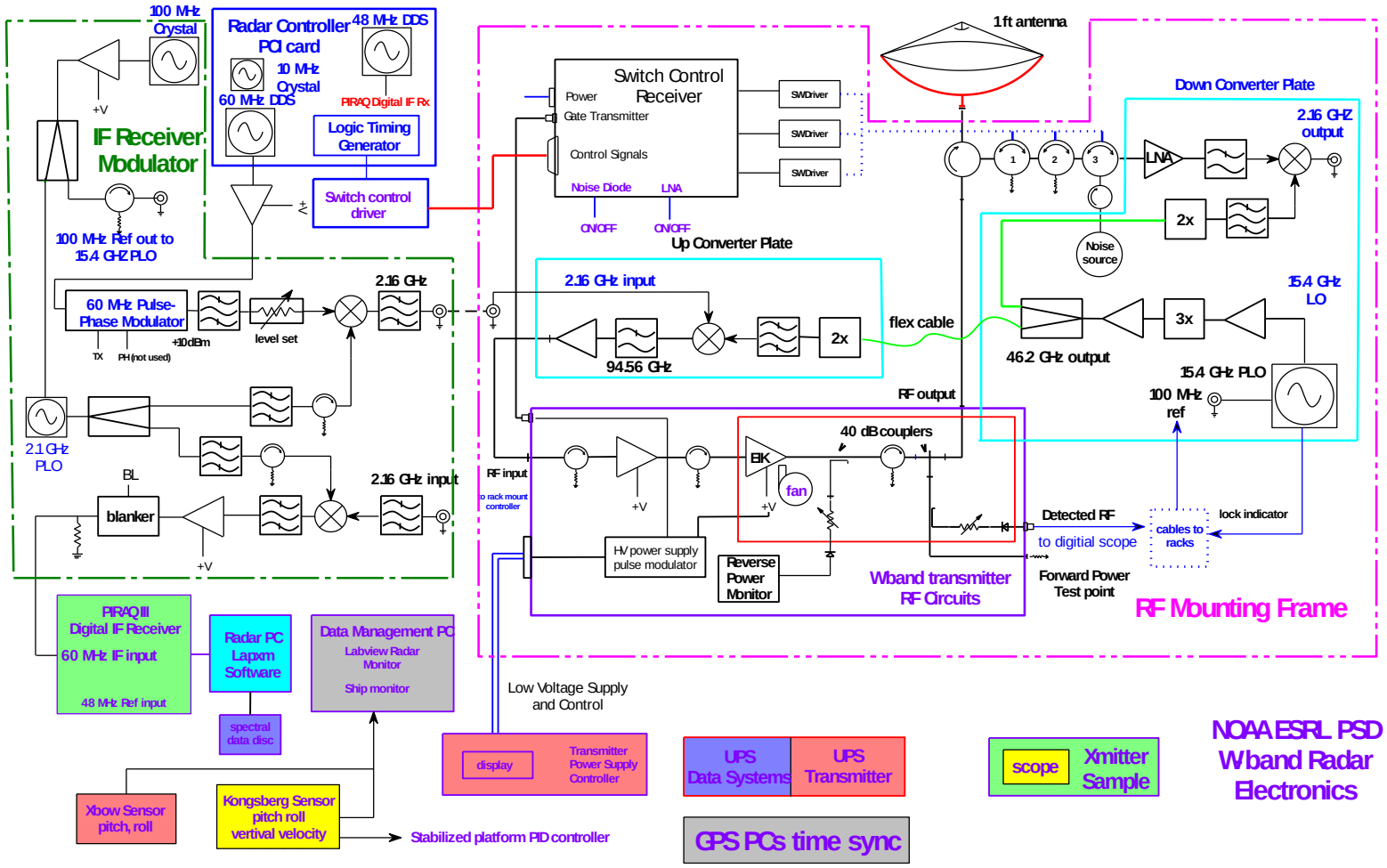
100 MHz Crystal
Radar Controller PCI card
48 MHz DDS
10 MHz Crystal
60 MHz DDS
PIRAQ Digital IF Rx
Logic Timing Generator
Switch control driver
IF Receiver Modulator
100 MHz Ref out to 15.4 GHz PLO
60 MHz Pulse-Phase Modulator
+10dBm
level set
TX
PH (not used)
2.16 GHz
2.1 GHz PLO
BL
blanker
2.16 GHz input
PIRAQ III Digital IF Receiver
60 MHz IF input
48 MHz Ref input
Radar PC Lapxm Software
spectral data disc
Data Management PC
Labview Radar Monitor
Ship monitor
Xbow Sensor pitch, roll
Kongsberg Sensor pitch roll vertival velocity
Stabilized platform PID controller
Low Voltage Supply and Control
display
Transmitter Power Supply Controller
UPS Data Systems
UPS Transmitter
GPS PCs time sync
Switch Control Receiver
Power
Gate Transmitter
Control Signals
Noise Diode
LNA
ON/OFF
SWDriver
Up Converter Plate
2.16 GHz input
94.56 GHz
2x
flex cable
RF output
RF input
to rack mount controller
+V
EIK
fan
40 dB couplers
HV power supply pulse modulator
Reverse Power Monitor
Wband transmitter RF Circuits
1ft antenna
Down Converter Plate
2.16 GHz output
LNA
Noise source
2x
15.4 GHz LO
3x
46.2 GHz output
15.4 GHz PLO
100 MHz ref
Detected RF
to digitial scope
Forward Power Test point
cables to racks
lock indicator
RF Mounting Frame
scope
Xmitter Sample
NOAA ESRL PSD Wband Radar Electronics

**Figure 2**.

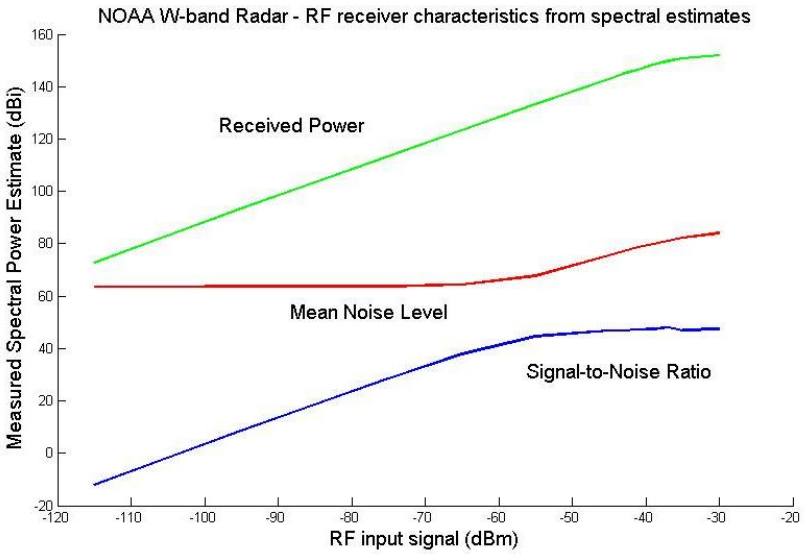
NOAA W-band Radar - RF receiver characteristics from spectral estimates
Measured Spectral Power Estimate (dBi)
RF input signal (dBm)
Received Power
Mean Noise Level
Signal-to-Noise Ratio
160
140
120
100
80
60
40
20
0
-20
-120
-110
-100
-90
-80
-70
-60
-50
-40
-30
-20

**Fig 3**

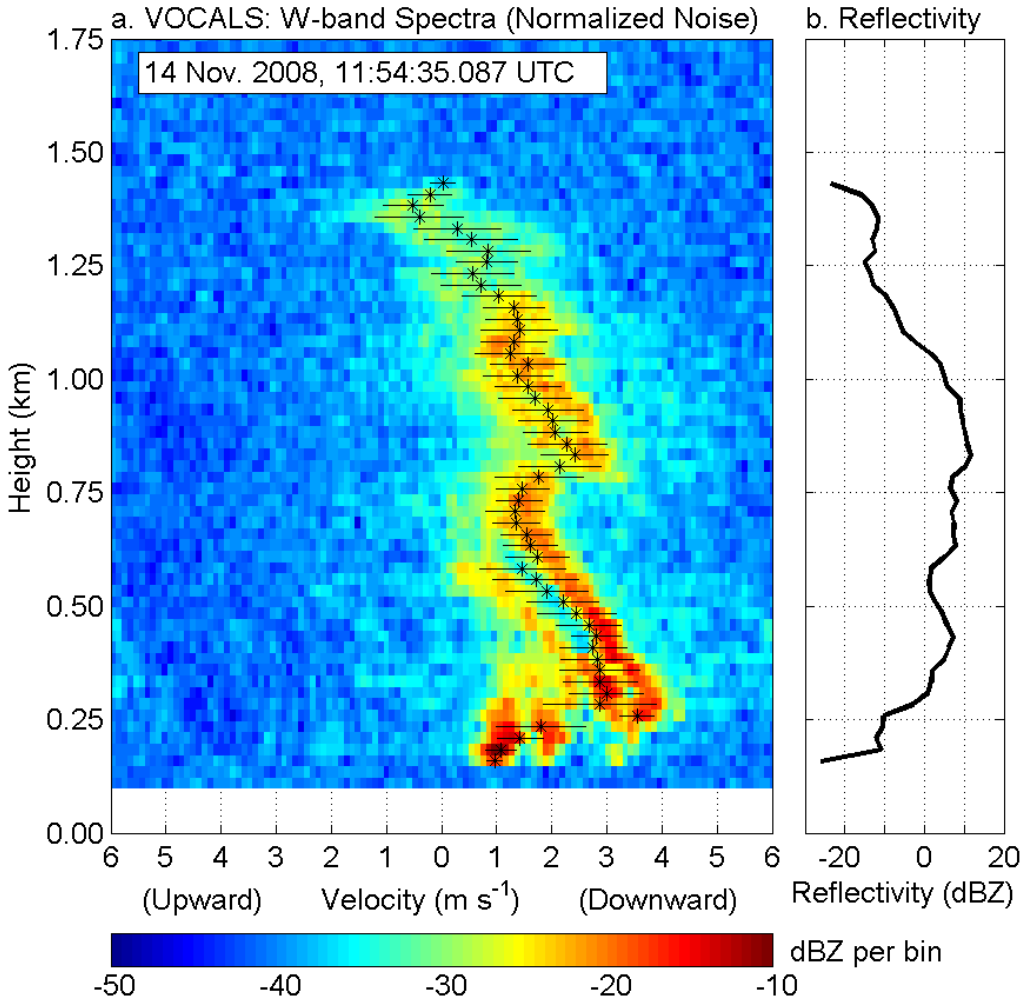
a. VOCALS: W-band Spectra (Normalized Noise)
b. Reflectivity
14 Nov. 2008, 11:54:35.087 UTC
Height (km)
1.75
1.50
1.25
1.00
0.75
0.50
0.25
0.00
6 5 4 3 2 1 0 1 2 3 4 5 6
(Upward) Velocity (m s-1) (Downward)
-20 0 20
Reflectivity (dBZ)
dBZ per bin
-50 -40 -30 -20 -10

**Fig 4a**

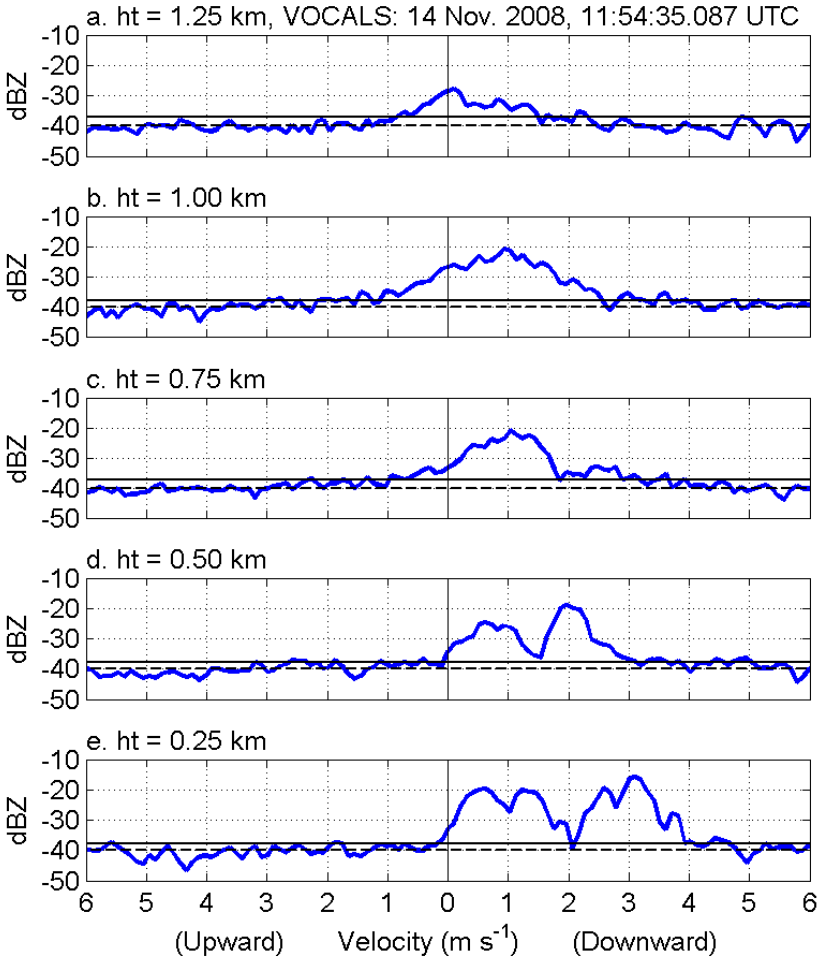
a. ht = 1.25 km, VOCALS: 14 Nov. 2008, 11:54:35.087 UTC
b. ht = 1.00 km
c. ht = 0.75 km
d. ht = 0.50 km
e. ht = 0.25 km
dBZ
-10
-20
-30
-40
-50
6 5 4 3 2 1 0 1 2 3 4 5 6
(Upward) Velocity (m s-1) (Downward)

**Fig 4b**

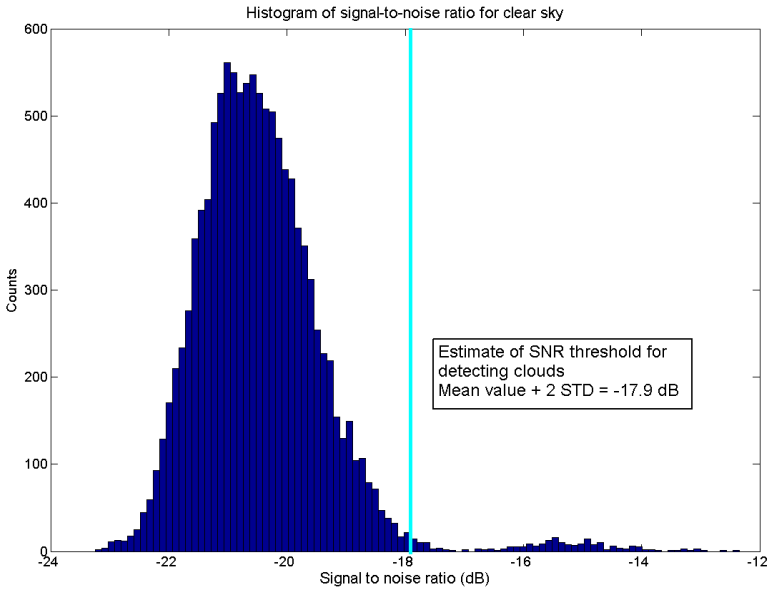
Histogram of signal-to-noise ratio for clear sky
Counts
Signal to noise ratio (dB)
Estimate of SNR threshold for
detecting clouds
Mean value + 2 STD = -17.9 dB

**Fig 5**

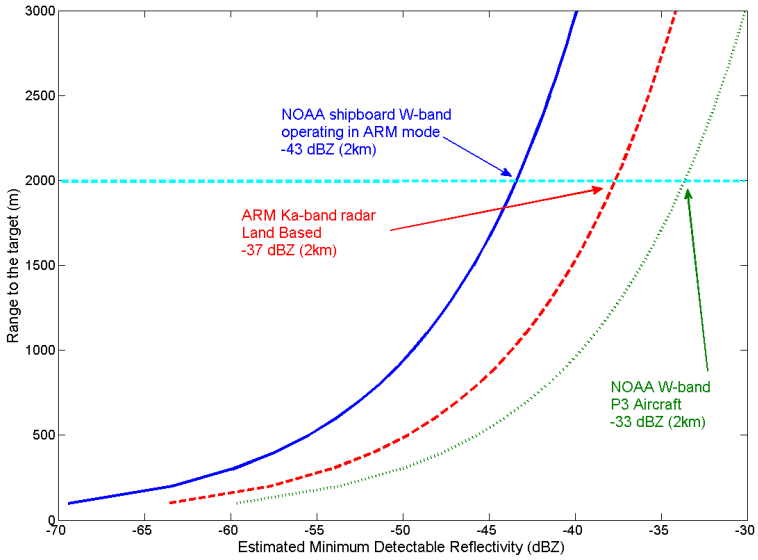
Range to the target (m)
Estimated Minimum Detectable Reflectivity (dBZ)
NOAA shipboard W-band
operating in ARM mode
-43 dBZ (2km)
ARM Ka-band radar
Land Based
-37 dBZ (2km)
NOAA W-band
P3 Aircraft
-33 dBZ (2km)

**Fig 6**

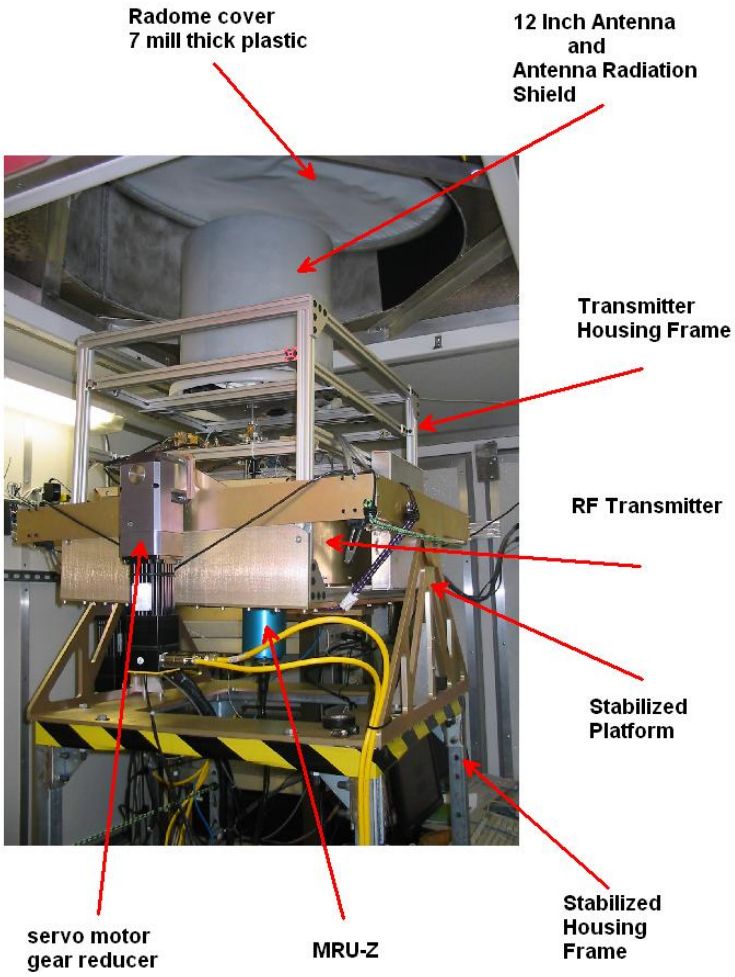
Radome cover
7 mill thick plastic
12 Inch Antenna
and
Antenna Radiation
Shield
Transmitter
Housing Frame
RF Transmitter
Stabilized
Platform
Stabilized
Housing
Frame
servo motor
gear reducer
MRU-Z

**Fig 7**

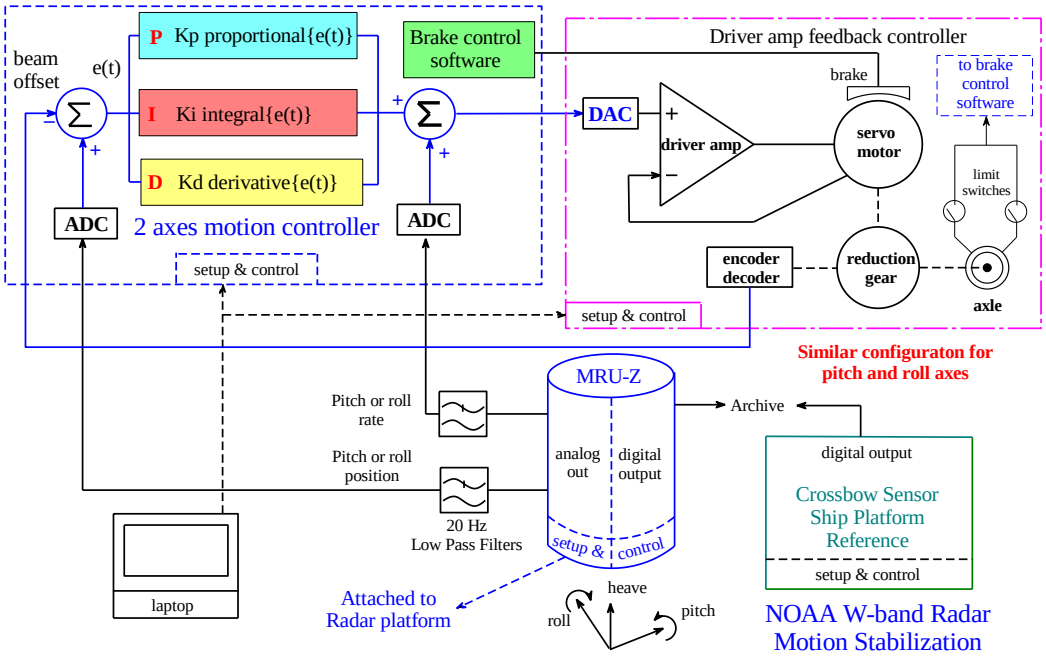
beam offset
e(t)
P Kp proportional{e(t)}
I Ki integral{e(t)}
D Kd derivative{e(t)}
Brake control software
ADC
2 axes motion controller
ADC
setup & control
Driver amp feedback controller
brake
to brake control software
DAC
driver amp
servo motor
limit switches
encoder decoder
reduction gear
axle
setup & control
Similar configuraton for pitch and roll axes
MRU-Z
Archive
Pitch or roll rate
Pitch or roll position
analog out
digital output
digital output
Crossbow Sensor Ship Platform Reference
setup & control
20 Hz Low Pass Filters
setup & control
laptop
Attached to Radar platform
heave
roll
pitch
NOAA W-band Radar Motion Stabilization

**Fig 8**

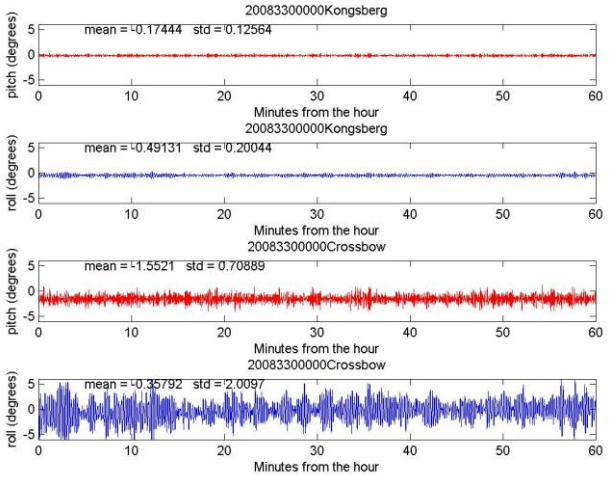
20083300000Kongsberg
mean = -0.17444 std = 0.12564
pitch (degrees)
Minutes from the hour
20083300000Kongsberg
mean = -0.49131 std = 0.20044
roll (degrees)
Minutes from the hour
20083300000Crossbow
mean = -1.5521 std = 0.70889
pitch (degrees)
Minutes from the hour
20083300000Crossbow
mean = -0.35792 std = 2.0097
roll (degrees)
Minutes from the hour

**Fig 9**

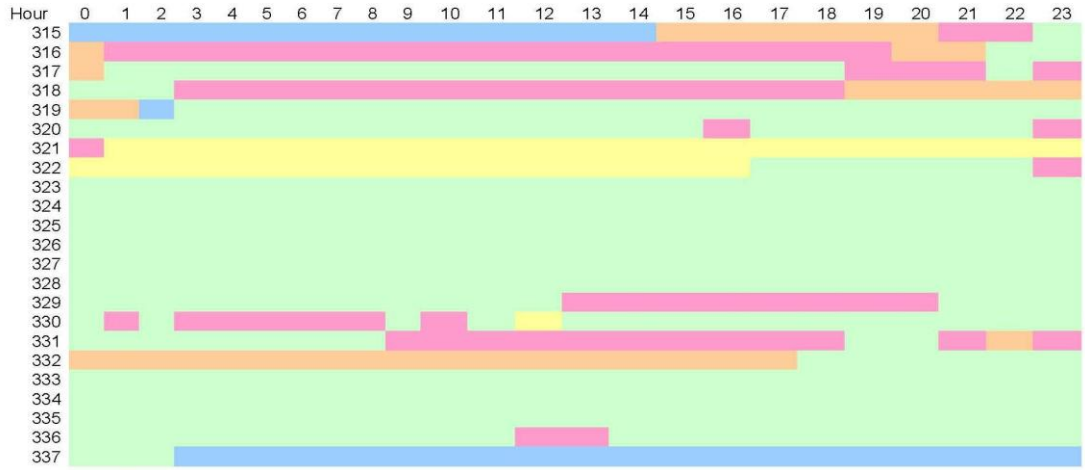
Hour
0 1 2 3 4 5 6 7 8 9 10 11 12 13 14 15 16 17 18 19 20 21 22 23
315
316
317
318
319
320
321
322
323
324
325
326
327
328
329
330
331
332
333
334
335
336
337

**Fig 10**

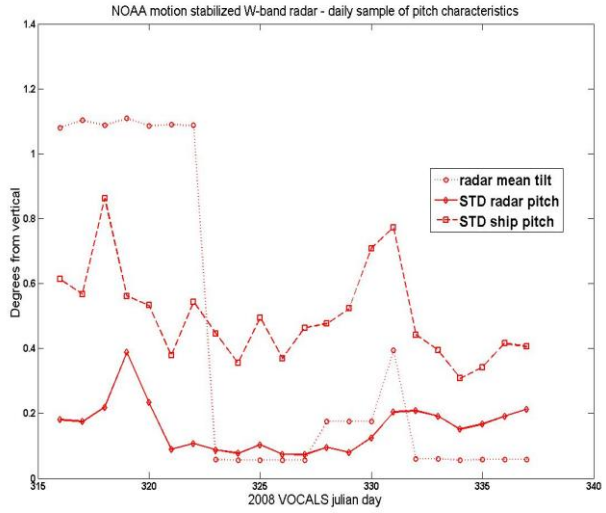
NOAA motion stabilized W-band radar - daily sample of pitch characteristics
Degrees from vertical
2008 VOCALS julian day
radar mean tilt
STD radar pitch
STD ship pitch

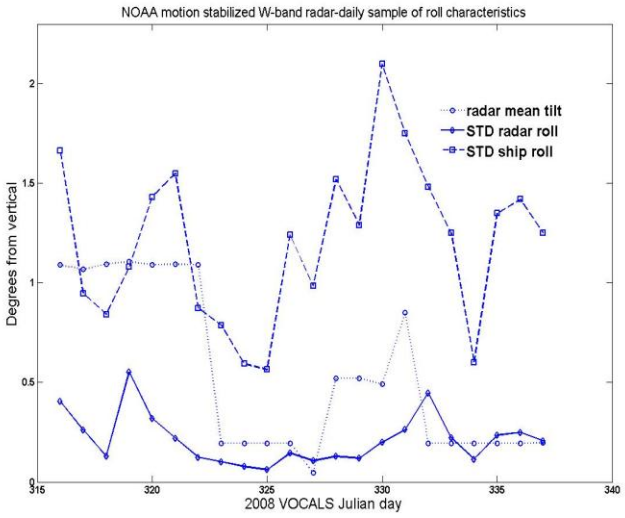
NOAA motion stabilized W-band radar-daily sample of roll characteristics
Degrees from vertical
2008 VOCALS Julian day
radar mean tilt
STD radar roll
STD ship roll

**Fig 11**

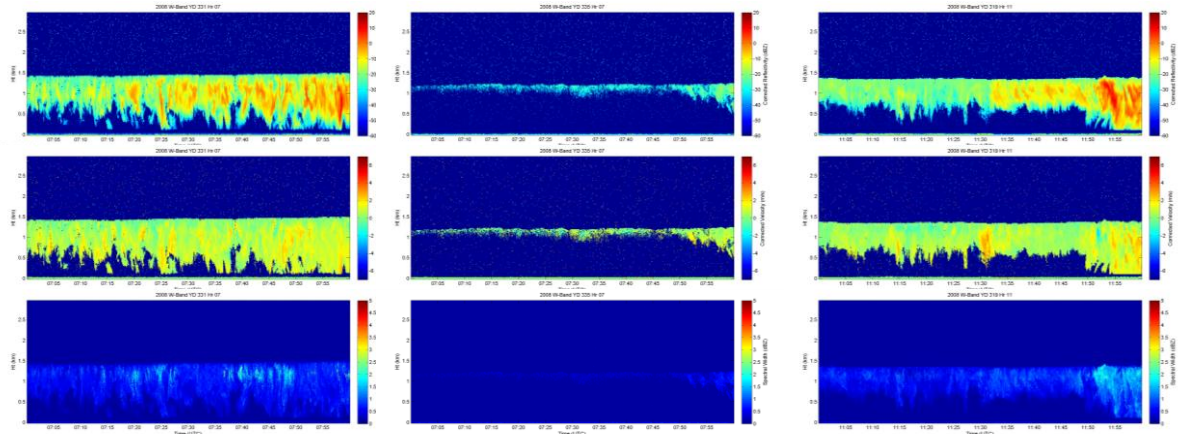

**Fig 12**

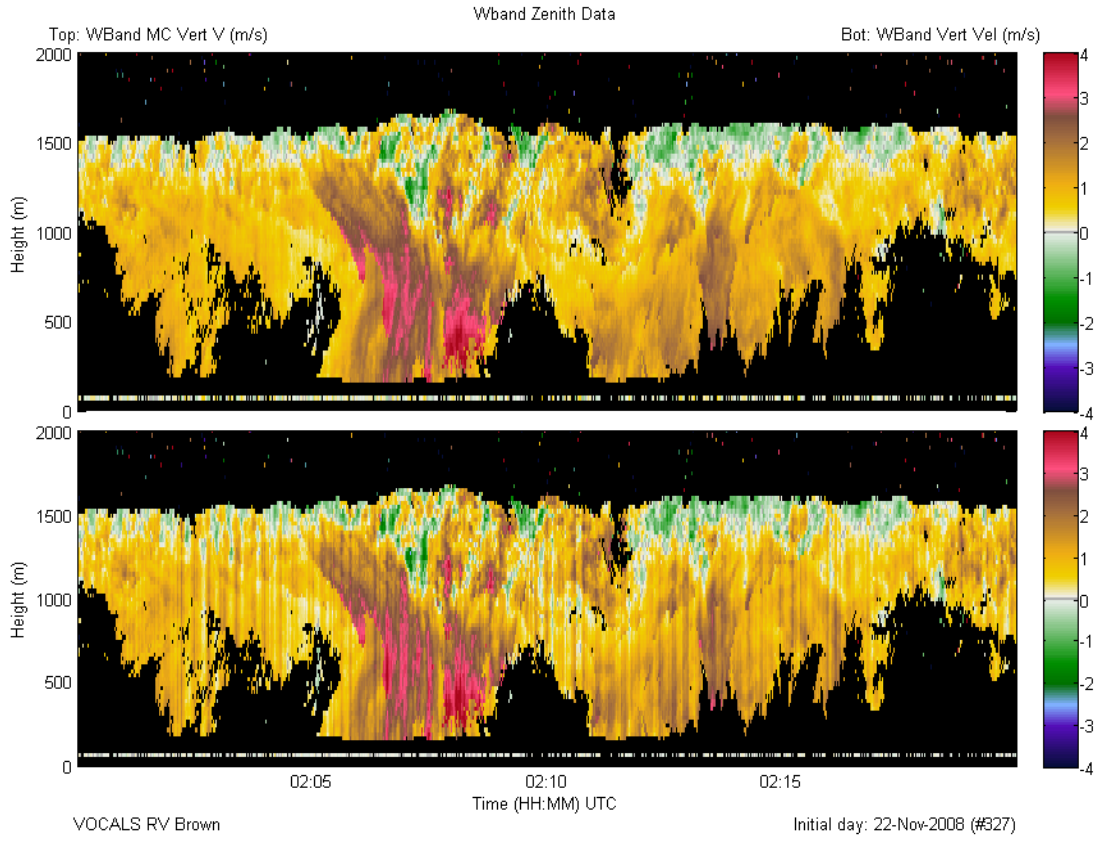
Wband Zenith Data
Top: WBand MC Vert V (m/s)
Bot: WBand Vert Vel (m/s)
Height (m)
2000
1500
1000
500
0
4
3
2
1
0
-1
-2
-3
-4
02:05
02:10
02:15
Time (HH:MM) UTC
VOCALS RV Brown
Initial day: 22-Nov-2008 (#327)

**Fig 13**

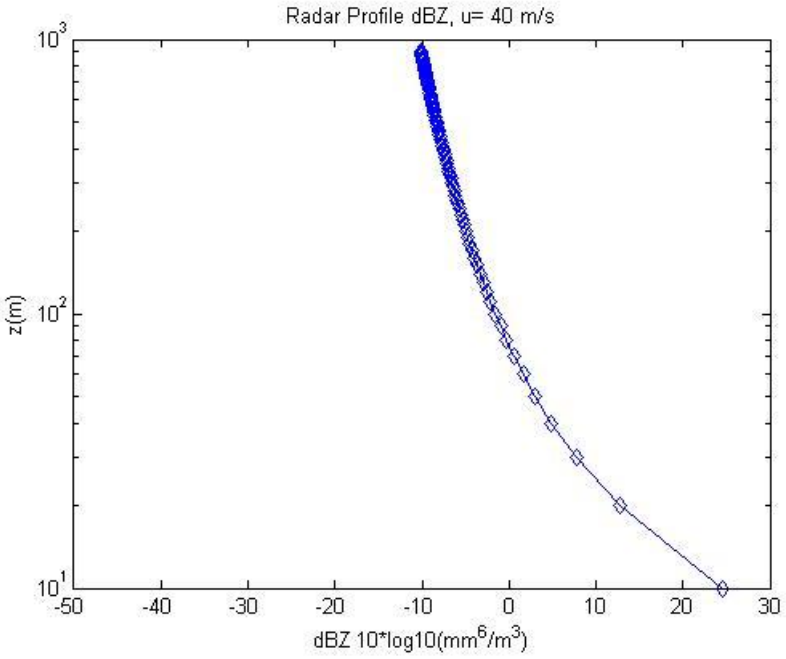
Radar Profile dBZ, u= 40 m/s
z(m)
$10^3$
$10^2$
$10^1$
-50
-40
-30
-20
-10
0
10
20
30
dBZ 10*log10(mm$^6$/m$^3$)

**Fig 14**

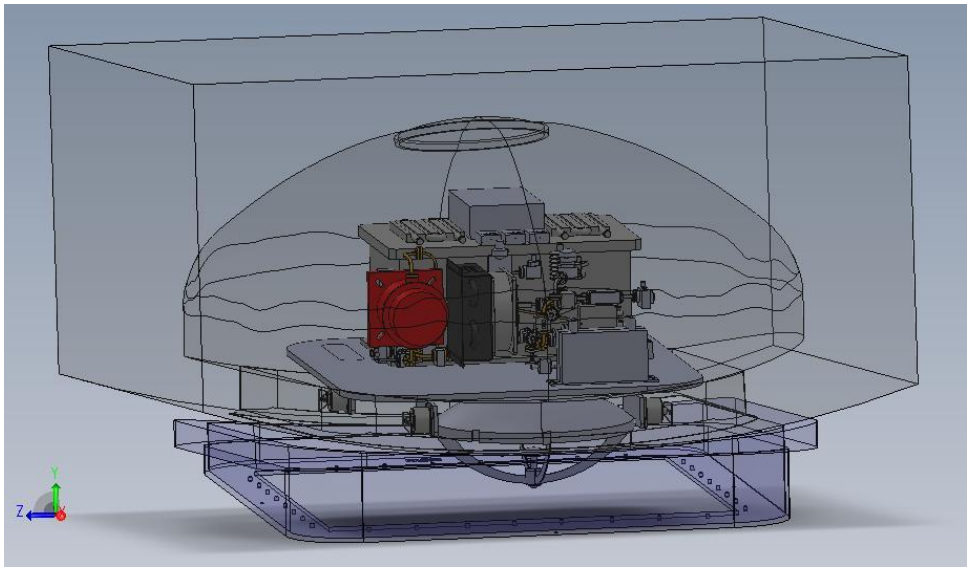

**Fig 15**